Journal of Controlled Release 320 (2020) 73–82

Contents lists available at ScienceDirect

Journal of Controlled Release

journal homepage: www.elsevier.com/locate/jconrel

A conductive cell-delivery construct as a bioengineered patch that can improve electrical propagation and synchronize cardiomyocyte contraction for heart repair

Shanglin Chen[a,b,1], Meng-Hsuan Hsieh[c,1], Shu-Hong Li[b], Jun Wu[b], Richard D. Weisel[b,d], Yen Chang[e], Hsing-Wen Sung[c,**], Ren-Ke Li[b,d,*]

[a] Department of Cardiac Surgery, Fuwai Hospital, National Center for Cardiovascular Diseases, Chinese Academy of Medical Sciences and Peking Union Medical College, Beijing, China
[b] Toronto General Hospital Research Institute, Division of Cardiovascular Surgery, University Health Network, Toronto, Canada
[c] Department of Chemical Engineering and Frontier Research Center on Fundamental and Applied Sciences of Matters, National Tsing Hua University, Hsinchu, Taiwan, ROC
[d] Division of Cardiac Surgery, Department of Surgery, University of Toronto, Toronto, Canada
[e] Taipei Tzu Chi Hospital, Buddhist Tzu Chi Medical Foundation and School of Medicine, Tzu Chi University, Hualien, Taiwan, ROC

ARTICLE INFO

Keywords:
Myocardial infarction
Cardiac arrhythmia
Conductive polymer
Electrical impulse propagation
Cardiomyocyte synchronization

ABSTRACT

Cardiac tissue engineering is of particular importance in the combination of contracting cells with a biomaterial scaffold, which serves as a cell-delivery construct, to replace cardiomyocytes (CMs) that are lost as a result of an infarction, to restore heart function. However, most biomaterial scaffolds are nonconductive and may delay regional conduction, potentially causing arrhythmias. In this study, a conductive CM-delivery construct that consists of a gelatin-based gelfoam that is conjugated with a self-doped conductive polymer (poly-3-amino-4-methoxybenzoic acid, PAMB) is proposed as a cardiac patch (PAMB-Gel patch) to repair an infarcted heart. A nonconductive plain gelfoam (Gel patch) is used as a control. The electrical conductivity of the PAMB-Gel patch is approximately 30 times higher than that of the Gel patch; as a result, the conductive PAMB-Gel patch can substantially increase electrical conduction between distinct clusters of beating CMs, facilitating their synchronous contraction. *In vivo* epicardial implantation of the PAMB-Gel patch that is seeded with CMs (the bioengineered patch) in infarcted rat hearts can significantly enhance electrical activity in the fibrotic tissue, improving electrical impulse propagation and synchronizing CM contraction across the scar region, markedly reducing its susceptibility to cardiac arrhythmias. Echocardiography shows that the bioengineered conductive patch has an important role in the restoration of cardiac function, perhaps owing to the synergistic effects of its conductive construct and the synchronously beating CMs. These experimental results reveal that the as-proposed bioengineered conductive patch has great potential for repairing injured cardiac tissues.

1. Introduction

Cardiovascular diseases are the leading cause of death globally [1]. Following an acute myocardial infarction (MI), cardiomyocytes (CMs) are lost and replaced by fibrosis. The accumulation of fibrillary cross-linked collagen deposition in the myocardium and scar formation of the defect can result in extensive ventricular remodeling and progressive heart failure, which can cause cardiac death [2]. The nonconductive fibrotic scar tissue may electrically uncouple viable CMs in the infarct region, producing a proarrhythmic milieu [3]. The lack of electric connection between the healthy myocardium and the insulated CMs in the scar may also contribute to asynchronous ventricular contraction and may eventually lead to progressive functional decompensation and death [3]. Although early scar formation may prevent ventricular

* Correspondence to: R.-K. Li, Division of Cardiovascular Surgery, Toronto General Hospital Research Institute, University Health Network, Toronto, Ontario M5G 1L7, Canada.
** Correspondence to: H.-W. Sung, Department of Chemical Engineering, National Tsing Hua University, Hsinchu 30013, Taiwan.
E-mail addresses: hwsung@mx.nthu.edu.tw (H.-W. Sung), renkeli@uhnresearch.ca (R.-K. Li).
[1] The first two authors (C.L. Chen and M.H. Hsieh) contributed equally to this work. *To whom correspondence should be addressed: renkeli@uhnresearch.ca (R.K. Li) and hwsung@mx.nthu.edu.tw (H.W. Sung).

https://doi.org/10.1016/j.jconrel.2020.01.027
Received 4 November 2019; Received in revised form 8 January 2020; Accepted 15 January 2020
Available online 17 January 2020
0168-3659/

rupture, ventricular pressure may cause thinning and stretching of the scar, leading to fatal ventricular dilatation and dysfunction. Novel techniques are therefore required to prevent ventricular thinning and dilation as well as to connect insulated contracting CMs and secure their synchronized contraction, ultimately preventing congestive heart failure.

In the last decade, cardiac tissue engineering has attracted much attention, especially with respect to the combination of contracting cardiac cells with a biomaterial scaffold as a cell delivery construct to replace cells that are lost as a result of an infarction and thereby to prevent ventricular dilation and restore heart function [4]. This delivery technique has the advantage of introducing very many cardiac cells, which can be grown in three dimensions to generate a thick functioning bioengineered cardiac patch. Collagen, gelatin, and fibrin are natural biomaterials and their structure is similar to the extracellular matrix, which can support a bioengineered cardiac patch when implanted with CMs [5–7].

In an earlier study, we used a gelatin-based gelfoam as a scaffold to generate a bioengineered cardiac patch that was seeded with CMs to repair an infarcted heart [6,8]. Gelfoam is an FDA-approved hemostatic sponge, which is mainly composed of cross-linked gelatin [9]. This three-dimensional, porous biomaterial scaffold can provide a suitable surface for cell attachment, increasing the number of surviving CMs and reducing the number of cells lost as a result of anoikis. Subsequently, we formed a cytokine-enhanced cardiac patch by immobilizing vascular endothelial growth factor and basic fibroblast growth factor into the gelfoam scaffold and then seeding it with human mesenchymal stromal cells [10]. This cytokine-enhanced, cell-seeded biodegradable patch prolonged cell survival and augmented angiogenesis. Rats that were implanted with this patch exhibited better cardiac function after surgical ventricular reconstruction; however, this advanced patch lacked conductive properties. Implantation of a nonconductive patch may impede electrical impulse propagation across the infarcted heart and is not able to electrically synchronize isolated contracting CMs within the scar area [11].

The electrical integration of a tissue-engineered construct with the native myocardium as well as the appropriately timed activation of contraction of CMs in response to stimulation may markedly enhance the contribution of the patch to the propulsion of blood out of the heart. To achieve this goal, this work proposes a novel cell delivery construct that consists of a conductive biomaterial scaffold that is made of a conductive polymer (poly-3-amino-4-methoxybenzoic acid, PAMB)-grafted gelfoam (PAMB-Gel patch) as a bioengineered cardiac patch for heart repair (Fig. 1). Its conductivity, ability to support CM viability and function *in vitro*, and effectiveness in the surgical repair of a myocardial infarct region *in vivo* are evaluated in detail.

2. Materials and methods

2.1. Preparation of PAMB-Gel patch

The PAMB-Gel patch was prepared by synthesizing the PAMB conductive polymer and conjugating it onto the backbone of gelatin that was present in the gelfoam (Ethicon, Somerville, NJ, USA) using an oxidative polymerization process [12]. Briefly, 3-amino-4-methoxybenzoic acid (AMB; Alfa Aesar, Ottawa, Canada) was dissolved in 10 mL deionized (DI) water (0 wt%, 0.5 wt%, 1.0 wt%, 2.0 wt%, or 4.0 wt%) in the presence of an oxidative catalyst (ammonium persulfate, APS) at an AMB to APS molar ratio of 1:1 at 40 °C. Samples of gelfoam (of length 15 mm, width 15 mm, and thickness 2 mm) were immersed in the as-prepared solutions and then reacted for 12 h at 40 °C. The PAMB-Gel patches thus formed were thoroughly washed in phosphate-buffered saline (PBS); the patch that had the highest conductivity was used in subsequent studies. Plain gelfoam (Gel patch) was used as a control.

2.2. Characterization of PAMB-Gel patch

The conjugation of PAMB into the patch was investigated by Fourier-transform infrared spectroscopy (FT–IR, Thermo Scientific, Nicolet iS50, Madison, WI, USA). The amount of PAMB that was conjugated into the patch was determined by measuring the absorbance of the patch at 500 nm using a UV–vis spectrophotometer (SpectraMax M5 Microplate Reader, Molecular Devices, Sunnyvale, CA, USA) [13].

The morphology of the Gel and PAMB-Gel patches was investigated by scanning electron microscopy (SEM, SU8010, Hitachi, Japan). ImageJ was used to analyze the obtained SEM micrographs to determine the mean pore size of each test patch, while its porosity was measured in pure ethanol by a liquid displacement method that has been described elsewhere [14]. The tendency of each test patch to swell was evaluated by immersing the dried test samples in PBS at 37 °C, and measuring their wet weights at the scheduled time points. The swelling ratio of each test patch was calculated using the following Eq. [15].

$$\text{Swelling Ratio} = (Ws–Wd)/Wd$$

where Ws and Wd are the weights of the swollen and dried samples, respectively.

The mechanical properties of the Gel and PAMB-Gel patches were elucidated using an Instron material testing machine (Model 5842, Norwood, MA, USA). The relevant experiments were performed with the machine in tensile mode at a constant crosshead speed of 5 mm/min [16]. The Young's modulus, tensile strength, and elongation at break were calculated from the obtained stress–strain curve. The self-doping characteristic of the PAMB conductive polymer at different pH values was evaluated by examining the UV–vis absorption spectrum of the polymer, which was obtained using a SpectraMax M5 Microplate Reader.

Conductivity was measured right after washing or soaking the patches in PBS for later measurement. The conductivities of the test patches were evaluated using a two-probe conductivity analyzer (Hewlett-Packard Development Company, Palo Alto, CA, USA). The 15 × 15 × 5 mm patches were placed on a platform and two probes at 7 mm distance from each other were used for conductivity measurements using a linear double-sweep model. The voltage increased from −5.0 to 5.0 V in 100 mV increments (delay time 100 μsec). The conductivity was calculated according to the slopes. The measurements were made in PBS.

2.3. Animal studies

Test rats (Sprague–Dawley; neonatal or adult weighing 200–250 g) were acquired from Charles River Laboratories (Saint-Constant, QC, Canada). All experimental procedures were conducted consistent with the Guide for the Care and Use of Laboratory Animals (NIH, 8th Edition, 2011), and the study protocols were approved by the Animal Research Centre of the University Health Network.

2.4. Preparation of cell-delivery construct (cell-seeded PAMB-Gel patch)

CMs were isolated from neonatal rats using enzymatic dissociation [17]. To reduce contaminating cardiac fibroblasts, the isolated cells were pre-seeded on a non-coated dish for 30 min. To prepare the cell delivery constructs, test patches (Gel and PAMB-Gel) were sterilized by UV for 30 min. The sterilized patches were firstly soaked in fetal bovine serum (FBS) for one hour and then in a 1:1 DMEM and Ham F12 (Life Technologies, Burlington, ON, Canada) medium that contained 10% FBS (DMEM/Ham F12 + 10% FBS) for another hour. The isolated CMs were plated at 2 × 10^6/patch in a DMEM/Ham F12 + 10% FBS medium that contained 100 U/mL penicillin G and 0.1 mg/mL streptomycin. To prevent the growth of non-myocytes in the early stages of the experiment, BrdU (10 mM; Sigma Aldrich, St Louis, MO, USA) was added to the medium on the first day of the cell culture; thereafter,

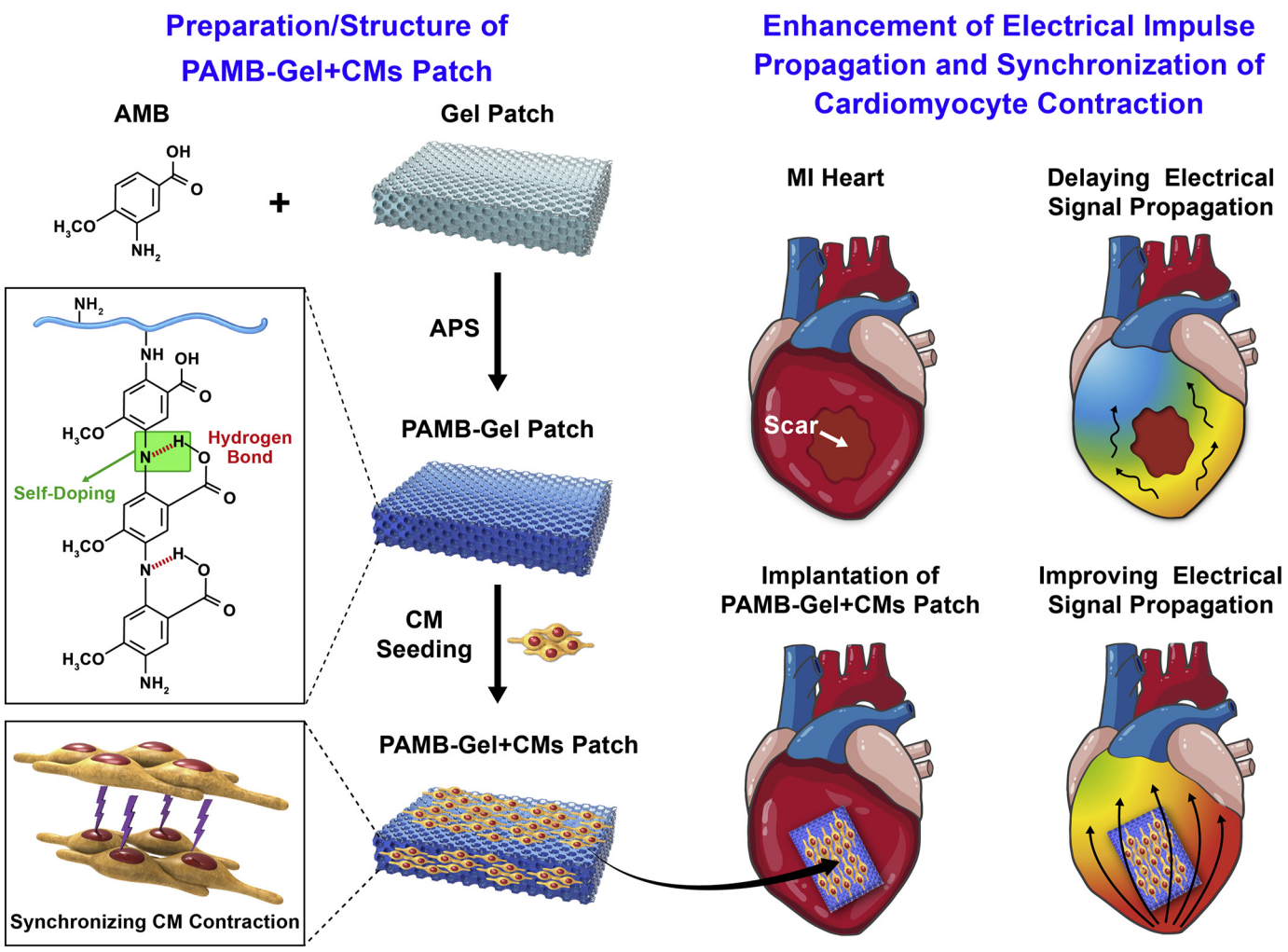

Fig. 1. Preparation and structure of as-proposed bioengineered conductive patch (PAMB-Gel + CMs) and mechanisms of its improvement of electrical propagation and synchronizing CM contraction for repair of infarcted rat heart.

BrdU was removed, and the cells were recultured in a medium that was the same except in that it contained 8% FBS. To evaluate cell viability in the as-prepared cell delivery constructs, the cultured cells were fixed in 2% paraformaldehyde for 10 min and permeabilized with 0.2% Triton X 100 for 5 min. Nuclei were counter-stained with 4′,6-diamidino-2-phenylindole (DAPI, Sigma Aldrich) and counted following two, four, six, or eight days in culture.

2.5. Immunofluorescent staining of cell-seeded PAMB-Gel patch

Immunofluorescent staining was carried out to detect the gap junction protein, connexin 43, on CMs that had been cultured in the test patches five days after seeding. The patches with cultured cells were fixed in 2% paraformaldehyde for 10 min, blocked in 5% donkey serum and then incubated with rabbit anti-connexin 43 (1:800; Sigma Aldrich, c6219), followed by Alexa546 donkey anti-rabbit IgG secondary antibody (1:400; Life Technologies). Nuclei were counter-stained with DAPI.

2.6. Conductive properties of cell-seeded PAMB-Gel patch

The conductive properties of the cell-seeded patches were investigated *via* extracellular electrical potential mapping with a specifically designed microelectrode array (MEA) system (Multichannel Systems, Reutlingen, Germany) [18]. The patches that had been seeded with CMs as described above were plated onto the MEA that covered the electrode grid at the center of a Petri dish. A MEA1060-Inv-BC System amplifier with a recording system (Multichannel Systems) was used to record the electrical activity of the cell-seeded test patch. The activation time at each recording site was identified by the sharp negative deflection. The electrical conduction velocity was measured by plotting activation time *versus* distance from the electrodes along the trajectory of propagation.

2.7. CM Ca^{2+} transient and electrical impulse propagation

CM Ca^{2+} transient propagation was assessed by incubating cell-seeded patches with the Ca^{2+} indicator dye Fluo-4 AM (acetoxymethyl; 5 μM) in enhancing medium Pluronic® F-127 for 30 min and then washing in fresh Tyrode's solution. Ca^{2+} transient propagation in CMs was detected by excitation with Fluo-4 AM at 488 nm and emission at > 515 nm. The area where CMs first demonstrated an increase in Ca^{2+} concentration was taken as region of interest (ROI) #1, and the area of the CMs where the propagation ended was taken as ROI #2. The time for propagation was that between the activation of ROI #1 and ROI #2. The distance between ROI #1 and #2 was measured and calculated using Image J software. The Ca^{2+} conduction velocity was calculated using a standard formula [conduction velocity = distance between the two ROIs/propagation time] [19].

Electrical impulse propagation through the left ventricle (LV) of the heart was optically mapped. The electrical signal conduction kinetics of the *ex vivo* Langendorff-perfused rat hearts [20] were investigated by

perfusing rat hearts with 10 μM of a voltage-sensitive dye, di-4-ANEPPS (Life Technologies), diluted in a high-potassium cardioplegia solution. Di-4-ANEPPS was excited at 510 nm, and its emission at > 570 nm was collected.

Ca^{2+} transient propagation in CMs and the electrical signal conduction kinetics of Langendorff-perfused hearts were recorded by an optical high-speed electron multiplied charge-coupled device (EMCCD) camera system (Evolve 128, Photometrics, Tucson, AZ, USA) that was coupled with a dissecting microscope. To record the electrical signals from the Langendorff-perfused rat hearts, the infarct scar was positioned in the center of the view. The measurement began when the first electrical signal appeared on the heart; this time was marked as zero. The end point was when the electrical signal propagation ended. The recorded fluorescence images were processed using a 100 Hz low-pass filter, pseudocolored, and then stacked to make isochronal maps of electrical signal propagation over time [21].

2.8. Epicardial implantation of cell-seeded PAMB-Gel patch and analysis of its electrical activity

Test rats underwent left descending coronary artery ligation to create the MI model. One week later, three groups of patches (Gel, PAMB-Gel, and PAMB-Gel + CMs) were separately sutured onto the epicardial surfaces of the infarct areas. The regional field potential amplitude of the fibrotic tissue four weeks after patch implantation was measured with a 36-lead flexible MEA. The global fibrotic scar tissue field potential amplitude was evaluated by an eight-lead electrocardiography (ECG) catheter. Telemetry ECG was used to record the spontaneous premature ventricular contractions (PVCs) or ventricular tachycardia (VT) four weeks after patch implantation, and the number of arrhythmias per hour was calculated [22].

Arrhythmias can be induced by various stimuli using an external stimulator [23]. A standard clinical programmed electrical stimulation (PES) protocol was applied to determine the inducibility of arrhythmias, which was quantified and presented as inducibility quotient, consistent with an established scoring system [24].

2.9. Cardiac function assessment and histological evaluation

Echocardiography (echo) was used to assess cardiac function. One week after MI, echo was performed, and only those rats whose hearts exhibited a fractional shortening of between 25 − 35% were included in the study. The cardiac function of the test rats was evaluated weekly using a GE Vivid 7 ultrasound system (GE Healthcare, Mississauga, ON, Canada) with a 10S transducer. Short-axis views were obtained using the parasternal method. LV dimensions (left ventricular end-diastolic internal diameter, LVIDd, and end-systolic internal diameter, LVIDs) were measured in M-mode. The ejection fraction was calculated as $(LVIDd^3 - LVIDs^3)/LVIDd^3 \times 100$. The fractional shortening was calculated as $(LVIDd - LVIDs)/LVIDd \times 100$. All echo traces were evaluated by a blinded researcher using echo analysis software (Millar, Houston, TX, USA).

At the end of the study (four weeks post-patch implantation), the hearts were arrested and fixed at physiological pressures. These fixed hearts were cut into 2-mm sections and photographed for morphometry. The infarct area was defined as the entire area of LV that was scarred in myocardial sections that were stained with Masson's trichrome. Scar thickness was measured by computerized planimetry and presented as an average of wall thickness measurements that were made at the middle and at each edge of the scar area at its thinnest point. All morphometric analyses were performed blind.

2.10. Statistical analysis

All collected data were analyzed using Prism version 7.0 software (GraphPad Software, San Diego, CA, USA) and were presented as mean ± SD. Student's *t*-test was used to make two-group comparisons. Comparisons of parameters among three or more groups were analyzed by one-way analysis of variance (ANOVA) for single-factor variables followed by Tukey or two-way ANOVA for two-factor variables with repeated measures over time, followed by Bonferroni *post-hoc* tests. Differences were regarded as statistically significant at $P < 0.05$.

3. Results and discussion

After an extensive MI, loss of CMs results in congestive heart failure. The replacement of the lost cells by the transplantation of a large number of beating CMs into the damaged area has attracted considerable attention [25]. However, methods of cell delivery into the myocardial tissue, including *via* transvenous [26], endomyocardial [27], or intracoronary [28] routes, have not been found to be entirely satisfactory as engraftment and cell survival have been limited [29], raising major challenges for clinical applications. In this study, a PAMB-grafted gelatin-based gelfoam is proposed as a conductive CM-delivery construct to support the formation of a synchronously beating cardiac tissue to repair an infarct heart. The absorbable gelatin sponge contains an essential component of the extracellular matrix, providing a unique biological environment that facilitates CM engraftment and cell survival.

3.1. Characteristics of PAMB-Gel patch

To form an electrically conductive patch, an oxidative catalyst (APS) was used to oxidize the nucleophilic amine groups on AMB monomers for generating polymerized PAMB; meanwhile, the polymerized PAMB was conjugated onto the gelatin backbone that was present in the gelfoam [30]. A three-dimensional, porous, conductive PAMB-Gel patch, was thus formed. Unmodified gelfoam (Gel patch) was used as a control patch. In the optimization of the formulation of the PAMB-Gel patch, the conductivity of the as-prepared patch increased with the AMB concentration, reaching a plateau at 2 wt% of AMB (Fig. 2a); further increasing the AMB concentration did not significantly increase the conductivity of the PAMB-Gel patch. Therefore, the patch that was prepared at an AMB concentration of 2 wt%, which had the highest conductivity of any the as-prepared patches, was chosen in the subsequent studies.

According to Fig. 2b, the FT–IR spectrum of the PAMB-Gel patch included two characteristic peaks at 1645 and 1540 cm^{-1} (indicated by the blue arrows), which were assigned to the amide I (C═O stretching vibration) and the amide II (N—H bending vibration) of gelatin (Gel patch), respectively. The peaks at 765 and 1020 cm^{-1} (red arrows) were attributed to the aromatic C—H out-of-plane bending vibration and the C–O–C stretching vibration of PAMB, respectively. These findings demonstrate that the AMB monomers had been successfully polymerized (PAMB) and conjugated onto the gelatin backbone. As verified using a UV–vis spectrophotometer [13], the amount of PAMB that was conjugated into the PAMB-Gel patch was 7.3 ± 0.2 wt% ($n = 6$ batches).

SEM was employed to observe the morphology of the Gel and PAMB-Gel patches. As presented in Fig. 2c, the Gel and PAMB-Gel patches exhibited similar three-dimensional, interconnected porous structures, and they had comparable pore sizes (210 μm) and porosities (80%) ($P > 0.05$, Fig. 2d and e). Patches with large pores and high porosity promote oxygen and nutrient exchange, which can favor cell attachment and growth [31].

The swelling properties of the Gel and PAMB-Gel patches were elucidated by measuring the variations of water contents in test samples that had been immersed in PBS. According to Fig. 2f, the conjugation of PAMB into the gelfoam slightly reduced its tendency to swell, potentially affecting the mechanical properties of the PAMB-Gel patch, as revealed by the obtained stress–strain curves in Fig. 2g. The PAMB-Gel patch had a higher Young's modulus, a greater tensile strength, and a

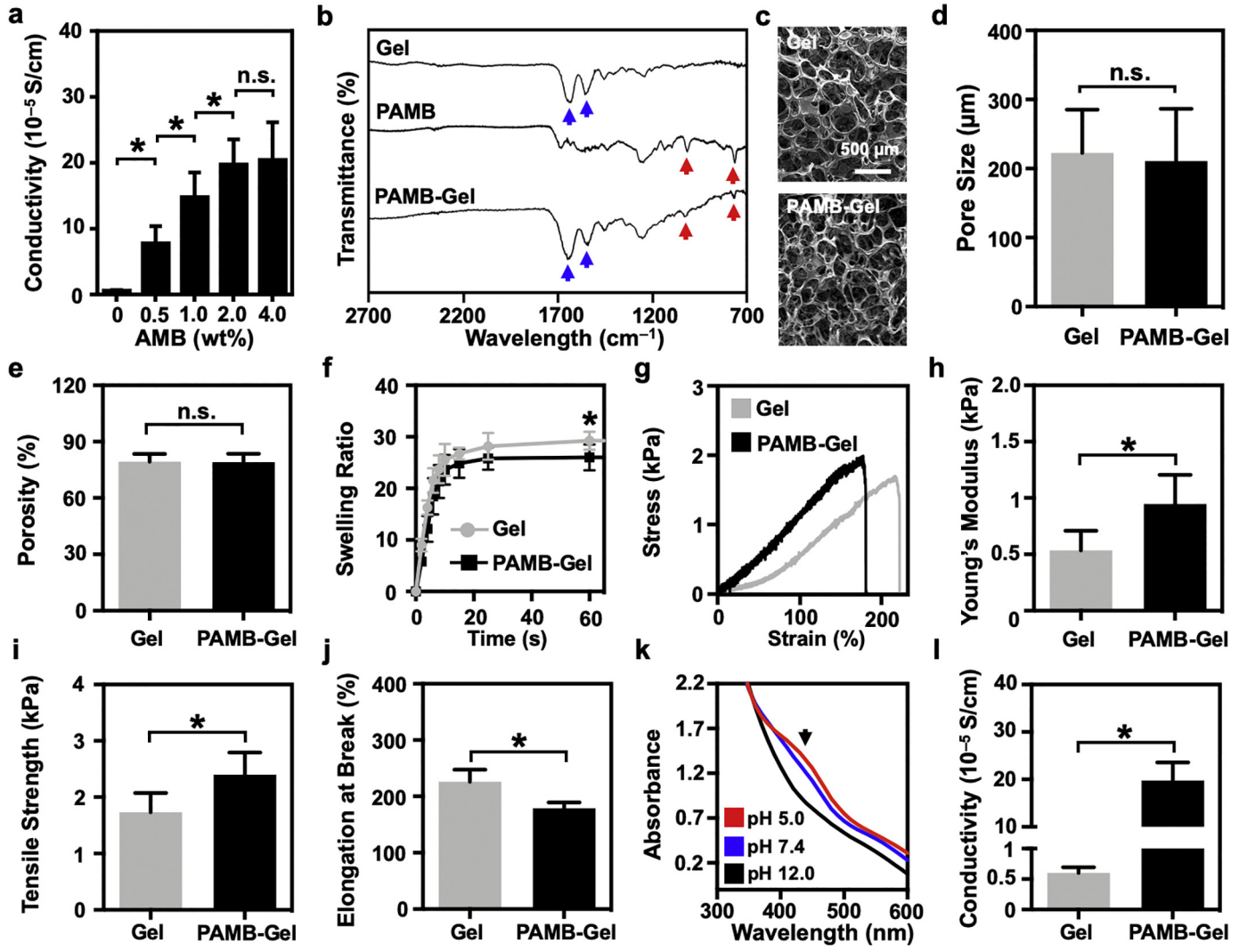

Fig. 2. (a) Conductivities of PAMB-Gel patches with various formulations ($n = 6$ in each group). (b) FT–IR spectra of Gel patch (gelfoam), PAMB polymer, and PAMB-Gel patch, indicating that PAMB polymer had been successfully synthesized and grafted into gelfoam. (c) SEM micrographs showing that Gel and PAMB-Gel patches had similar interconnected porous structures. (d) Pore size and (e) porosity of Gel and PAMB-Gel patches, suggesting that conjugation of PAMB did not change morphological structure of Gel patch ($n = 6$ in each group). (f) Swelling ratios of Gel and PAMB-Gel patches. (g) Stress–strain curves, (h) Young's moduli, (i) tensile strengths, and (j) elongations at break of Gel and PAMB-Gel patches (n = 6 in each group). (k) UV–vis absorption spectra of PAMB polymer at different pH values, showing self-doping at physiological pH. (l) Conductivities of Gel and PAMB-Gel patches (n = 6 in each group). *$P < 0.05$; n.s.: not significant.

lower elongation at break than the Gel patch (Figs. 2h–j). These experimental data reveal that the conjugation of PAMB renders the PAMB-Gel patch somewhat stiffer and mechanically stronger than the plain Gel patch, possibly owing to the rigid aromatic ring of PAMB and its relative hydrophobicity [32].

To explore the pH-responsiveness of its self-doping characteristic, the optical absorbances of the PAMB polymer at various pH values were recorded. Fig. 2k shows a broad absorption band at 420–440 nm in the UV–vis spectrum of PAMB at pH 5.0 and 7.4, which was generated by a polaron transition [33], revealing that the PAMB polymer had high conductivity. PAMB is a carboxyl group-functionalized polyaniline, which exhibits intra-molecular hydrogen bonding between the carboxyl group and the amino group in its repeating unit (Fig. 1). This intra-molecular hydrogen bonding reduces the electron density of the nitrogen, making the PAMB polymer self-doped at physiological pH (such as pH 5.0 and 7.4). When the environmental pH was increased to 12.0, the absorption band in the spectrum of PAMB was greatly repressed, owing to dedoping. These analytical results suggest that the as-prepared PAMB-Gel patch can be electrically active in a physiological pH environment. As confirmed using a two-probe conductive analyzer, at pH 7.4, the electrical conductivity of the conductive PAMB-Gel patch was approximately 30 times greater than that of the nonconductive Gel patch (Fig. 2l). The conductivity of the PAMB-Gel patch is 1.9×10^{-4} S/cm (Fig. 2l), which is within the conductivity range of the native myocardium (in the range of 5×10^{-5} to 1.6×10^{-3} S/cm) [34–36]. Therefore, the semi-conductive property of this material makes it a suitable candidate for cardiac repair. The successful conjugation of PAMB into the gelfoam may make it an ideal three-dimensional scaffold as a bioengineered cardiac patch with bioconductivity.

3.2. Cell compatibility of PAMB-Gel patch

To study the cell compatibility of the PAMB-Gel patch, neonatal rat CMs were isolated and grown in the test patch for eight days; the Gel patch was used as a control. Immunofluoresent staining was performed to identify the gap junctional protein, connexin 43, on CMs that had been cultured in the Gel and PAMB-Gel patches. According to Fig. 3a, connexin 43 proteins were clearly observed around the plasma membranes of the CMs (as indicated by the white arrowheads) that had been cultured in the Gel and PAMB-Gel patches. Similar numbers of CMs

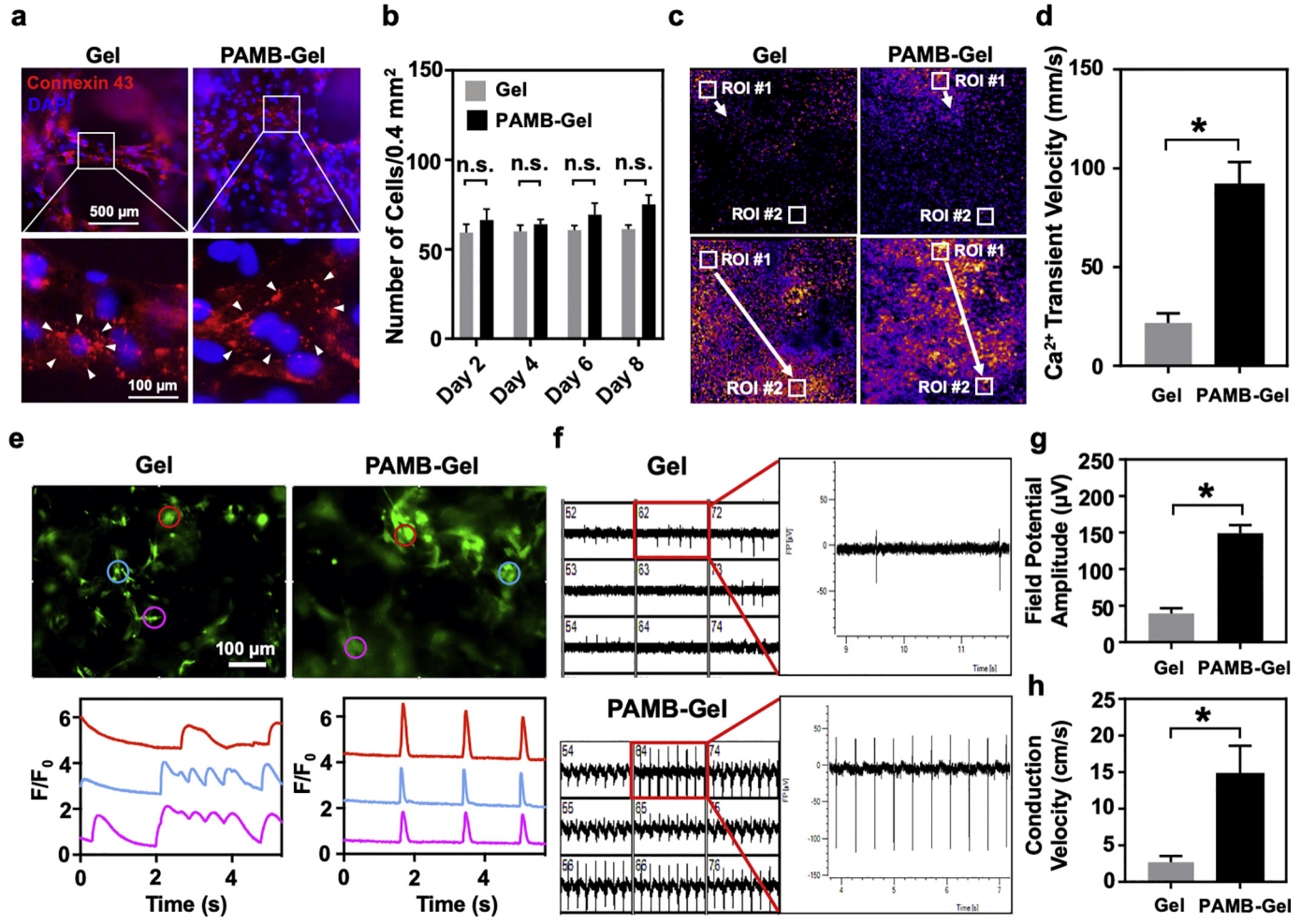

Fig. 3. (a) Representative fluorescence images of connexin 43 staining of CMs that had been grown in Gel and PAMB-Gel patches. Nuclei were counter-stained with DAPI. (b) Numbers of CMs grown in Gel and PAMB-Gel patches during eight days in culture ($n = 3$ in each group). (c) Ca^{2+} transient propagation through CMs that had been grown in Gel and PAMB-Gel patches. Area where Ca^{2+} fluorescence increased first was selected as ROI #1, and area where Ca^{2+} fluorescence propagation stopped was selected as ROI #2. (d) Ca^{2+} transient velocities in CMs that had been cultured in Gel and PAMB-Gel patches were calculated from time between activation of ROI #1 and that of ROI #2 (n = 3 in each group). (e) Ca^{2+} transients of distinct clusters of spontaneously beating CMs that had been grown in PAMB-Gel patch, exhibiting better synchronization than those that had been grown in Gel patch. (f) Representative electrograms of CMs that had been grown in Gel and PAMB-Gel patches, detected by MEA, showing that PAMB-Gel group had (g) higher field potential amplitude and (h) greater conduction velocity than Gel group (n = 3 in each group). *$P < 0.05$; n.s.: not significant.

grew in both studied patches during the eight days of culture ($P > 0.05$, Fig. 3b).

3.3. Ca^{2+} transient propagation in PAMB-Gel patch

To investigate the effect of the PAMB-Gel patch on the electrical conduction of cultured CMs, cytoplasmic Ca^{2+} transient propagation was determined by identifying the time between the activation of ROI #1 and that of ROI #2 (Fig. 3c). Fig. 3d indicates that the Ca^{2+} transient velocity of the CMs that were cultured in the conductive PAMB-Gel patch was about three times greater than that of the CMs that were grown in the nonconductive Gel patch ($P < 0.05$), indicating that the conjugation of conductive PAMB into the gelfoam (PAMB-Gel patch) significantly promoted Ca^{2+} transient propagation in the CMs.

Ca^{2+} transients of distinct clusters of spontaneously-beating CMs, which are related to CM contractions [37], were examined further in the Gel and PAMB-Gel patches. Three regions of the patches were randomly selected and their fluorescence intensities were analyzed. As displayed in Fig. 3e and Movie S1, the Ca^{2+} transients of the distinct clusters of CMs that had been grown in the PAMB-Gel patch showed better synchronization than those of CMs that had been grown in the Gel patch. These results reveal that the conductive PAMB-Gel patch can promote electrical conduction between distinct clusters of beating CMs, facilitating their synchronous contraction, and so may be used as a bioconductive cardiac engineered patch to restore infarcted hearts.

3.4. Electrical impulse propagation in CMs grown in PAMB-Gel patch

MEA was used to evaluate the regional field potential of CMs that had been grown in the Gel and PAMB-Gel patches. Conduction velocity was then calculated by observing the waveforms of two adjacent electrodes that were one mm apart; the delay times between the two waves were obtained from the graphs. According to Figs. 3f–h, the regional field potential amplitude that was generated from the CMs that had been cultured in the PAMB-Gel patch and its conduction velocity were both markedly greater than those generated from the CMs that had been grown in the Gel patch ($P < 0.05$), suggesting that the conductive PAMB-Gel patch enhanced the electrical impulse propagation in CMs.

3.5. Electrical impulse propagation in infarcted hearts

To translate the above favorable *in vitro* findings into potential

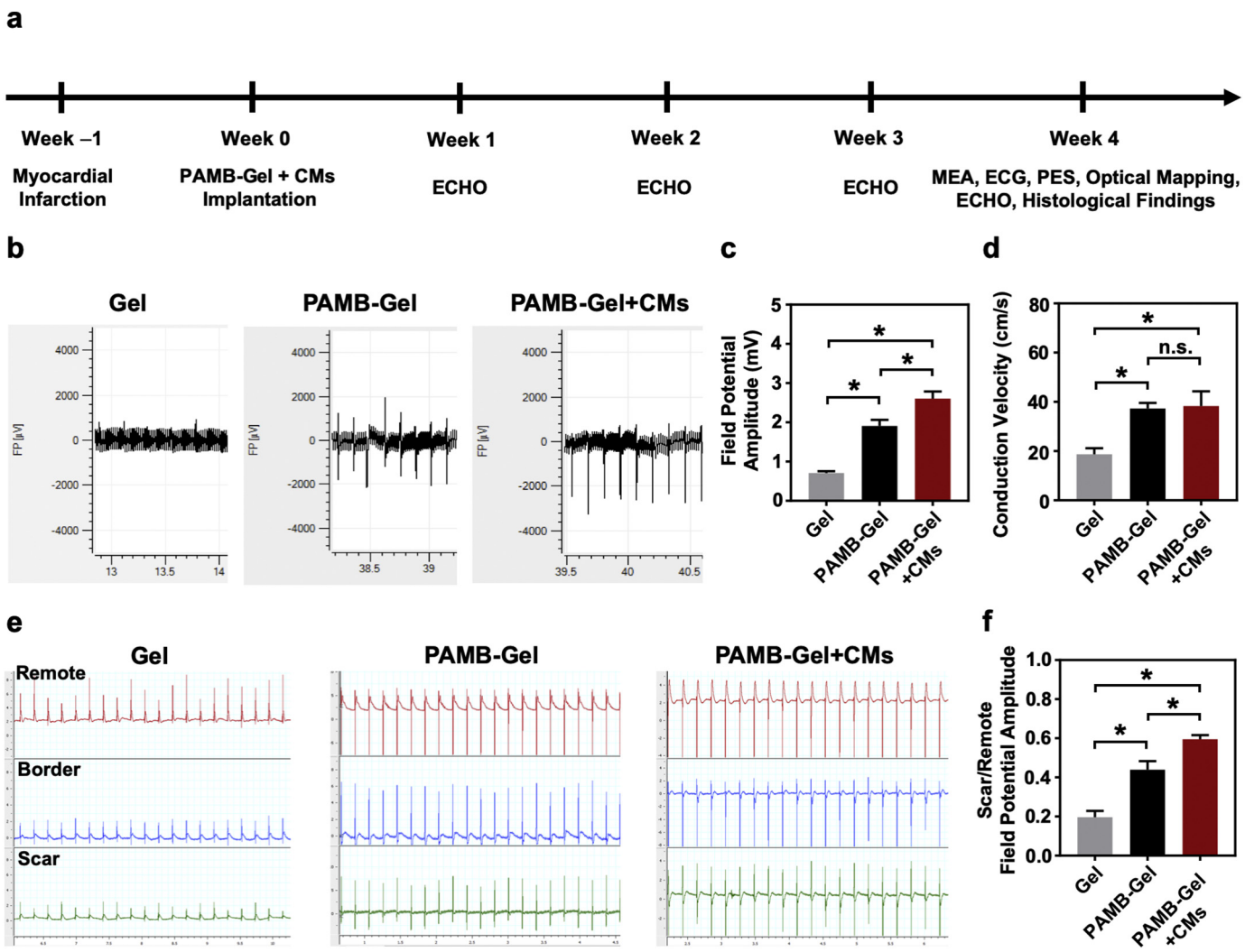

Fig. 4. (a) Experimental timeline. (b) Electrograms of regional field potential recorded on fibrotic scar areas using MEA and their (c) regional field potential amplitudes as well as (d) conduction velocities ($n = 6$ in each of Gel and PAMB-Gel groups; $n = 4$ in each of normal and PAMB-Gel + CMs groups). (e) Electrograms of global field potential recorded across fibrotic scar tissues using an eight-lead catheter and (f) corresponding ratios of scar/remote field potential amplitudes (n = 6 in each of Gel and PAMB-Gel groups, n = 4 in PAMB-Gel + CMs group). *$P < 0.05$; n.s.: not significant.

clinical applications, the effect of the PAMB-Gel patch that was seeded with CMs (PAMB-Gel + CMs or the bioengineered conductive patch) on cardiac repair and the resynchronization of electrical activity of the fibrotic scar tissue *in vivo* were evaluated using a rat MI model. The unseeded Gel and PAMB-Gel patches were used as controls. One week after the MI was created, epicardial implantation of each test patch was performed (Fig. 4a). Four weeks following patch implantation, MEA was used to evaluate the regional electrical field potential and electrical impulse propagation across the infarct scar area and an eight-lead catheter was used to measure the global field potential amplitude on the cardiac surface.

As indicated in Fig. 4b and c, the bioengineered conductive patch-treated infarcted hearts had the highest regional electrical field potential around the scar area of the three investigated groups of hearts ($P < 0.05$). The conduction velocity of the group that had received the PAMB-Gel patch significantly exceeded that in the rat hearts that had received the Gel patch (Fig. 4d, $P < 0.05$), possibly owing to the higher bioconductivity in the former group (Fig. 2l). The addition of CMs to the PAMB-Gel patch (bioengineered patch) did not increase regional conduction (Fig. 4d). The global field potential amplitude measurements revealed that the scar/remote field potential amplitude ratio in the group that was treated with the bioengineered patch significantly exceeded those observed in the groups that were treated with the Gel patch or the PAMB-Gel patch ($P < 0.05$, Fig. 4e and f). These analytical results suggest that epicardial implantation of the bioengineered conductive patch (PAMB-Gel + CMs) substantially improved electrical activity in the fibrotic tissue, promoting electrical impulse propagation and CM synchronization across the scar region.

3.6. QRS duration in infarcted hearts

Previous works have found that myocardial scars can cause "widened" QRS complexes [38]. To examine the effect of the treatment a conductive patch on QRS duration, surface ECG recordings were obtained four weeks after patch implantation (Fig. 4a). The QRS durations of infarcted hearts that were treated with a conductive patch (the PAMB-Gel patch or the bioengineered patch) were significantly shorter than that of the infarcted hearts that were treated with a non-conductive patch (the Gel-patch, $P < 0.05$, Fig. 5a and b). These experimental data indicate that the conductive PAMB-Gel patch enhanced regional as well as global conductions.

3.7. Inducibility of cardiac arrhythmias in infarcted hearts

In MI, the weakly excitable scar tissue impedes myocardial electrical propagation, potentially inducing macro re-entrant circuits and

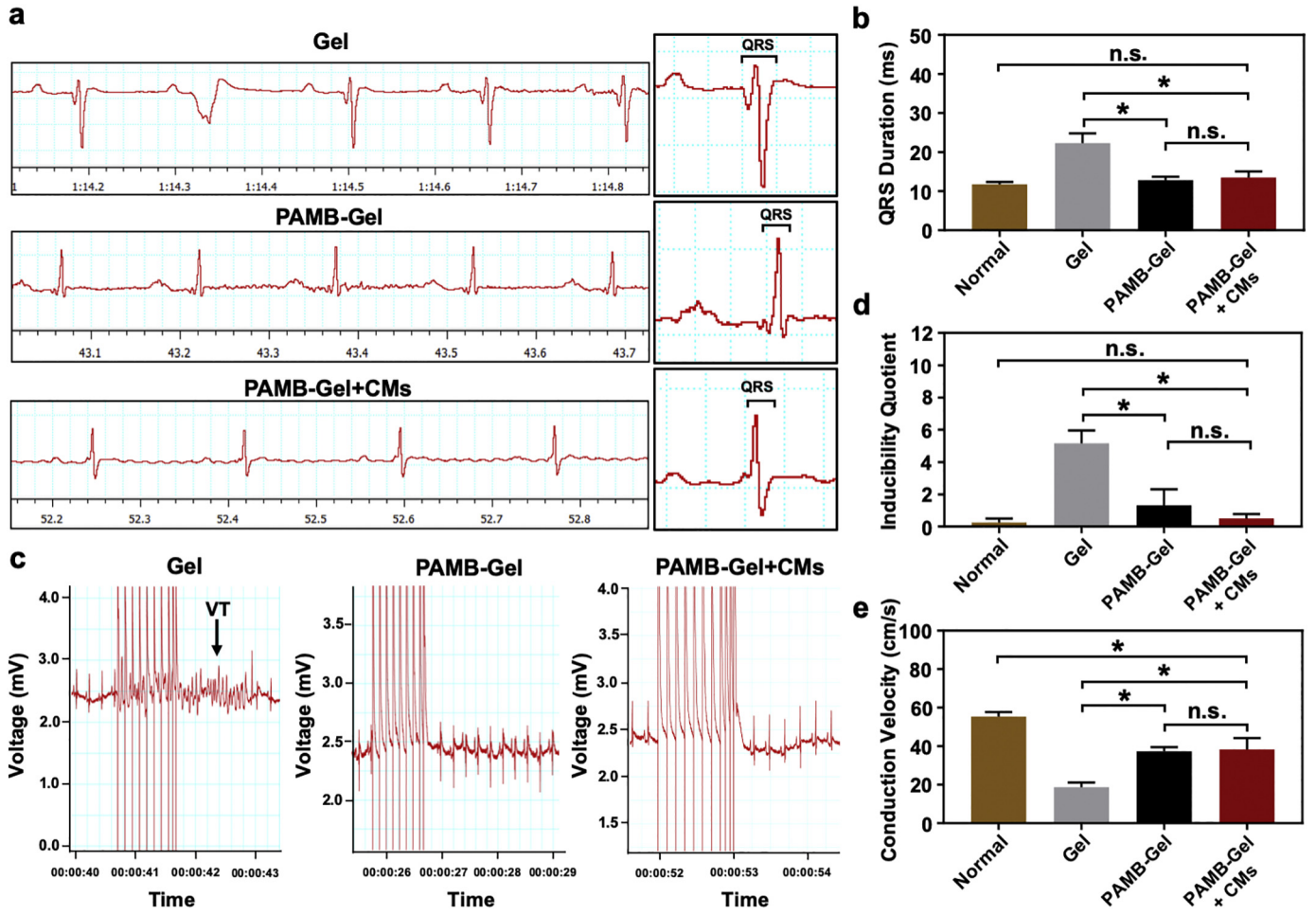

Fig. 5. (a) ECG recordings were taken to determine (b) QRS duration four weeks post-patch implantation ($n = 6$ in each of Gel and PAMB-Gel groups, $n = 4$ in each of normal and PAMB-Gel + CMs groups). (c) PES protocol was followed to investigate inducibility of arrhythmias of infarcted hearts. (d) Calculated inducibility quotients (n = 6 in each of Gel and PAMB-Gel groups, n = 4 in each of normal and PAMB-Gel + CMs groups). (e) Conduction velocities were calculated from optical mappings recorded at four weeks post-patch implantation (n = 6 in each of Gel and PAMB-Gel groups, n = 4 in each of normal and PAMB-Gel + CMs groups). *$P < 0.05$; n.s.: not significant.

ventricular arrhythmias [39]. To determine whether the epicardial implantation of a conductive patch onto the scar tissue may reduce its spontaneous cardiac arrhythmias, a standard clinical PES protocol was used [24]. According to Fig. 5c and d, when the infarcted hearts were challenged with PES, the susceptibility of cardiac arrhythmias was significantly lower, based on the calculated inducibility quotient, in the groups that had been implanted with the conductive PAMB-Gel patch, whether seeded with CMs (the bioengineered patch) or not, than in the group that had been implanted with the nonconductive Gel patch ($P < 0.05$,). This result suggests that the epicardial implantation of a conductive patch on an infarcted heart can substantially reduce its susceptibility to cardiac arrhythmias.

3.8. Electrical conduction velocity across infarcted hearts

Optical mapping was utilized to determine the conduction velocity of electrical impulse propagation across an infarcted heart that had been epicardially implanted with a test patch. At four weeks after implantation, hearts were excised and subsequently Langendorff-perfused with a voltage-sensitive dye (di-4-ANEPPS); the electrical conduction velocities across the normal and infarcted scar regions in each of the studied groups were then evaluated. Fig. 5e shows that the electrical conduction velocity in the groups that had been implanted with the PAMB-Gel patch or the bioengineered patch significantly exceeded that in the group that had been implanted with the Gel patch ($P < 0.05$). These findings suggest that the epicardial implantation of a conductive patch greatly improved electrical propagation across the repaired region, electrically activating isolated contracting regions to bridge the scar barrier to the healthy myocardium.

3.9. Cardiac function and histological findings

To assess whether the improved electrical impulse propagation (Figs. 3c, d, 4d, and 5e) and the synchronized CM contraction (Fig. 3e) that were observed in the group that had received the bioengineered conductive patch favored functional recovery, cardiac function was evaluated by echo every week following patch implantation. Cardiac function analyses demonstrate a relatively greater fractional shortening (Fig. 6a) and ejection fraction (Fig. 6b) and lower LVIDs (Fig. 6c, $P < 0.05$) and LVIDd (Fig. 6d) in the infarcted heart that had been treated with the bioengineered conductive patch than in the infarcted hearts that had been treated with the Gel patch or the PAMB-Gel patch. These results reveal that the bioengineered patch can importantly promote the restoration of cardiac function after MI, perhaps owing to the synergistic effects of its conductive construct and the synchronously beating CMs.

Trichrome staining shows that at four weeks after implantation, the infarcted heart that had been treated with the Gel patch had thinned, whereas those had been treated with the PAMB-Gel patch or the bioengineered patch, each of which was structurally integrated with the

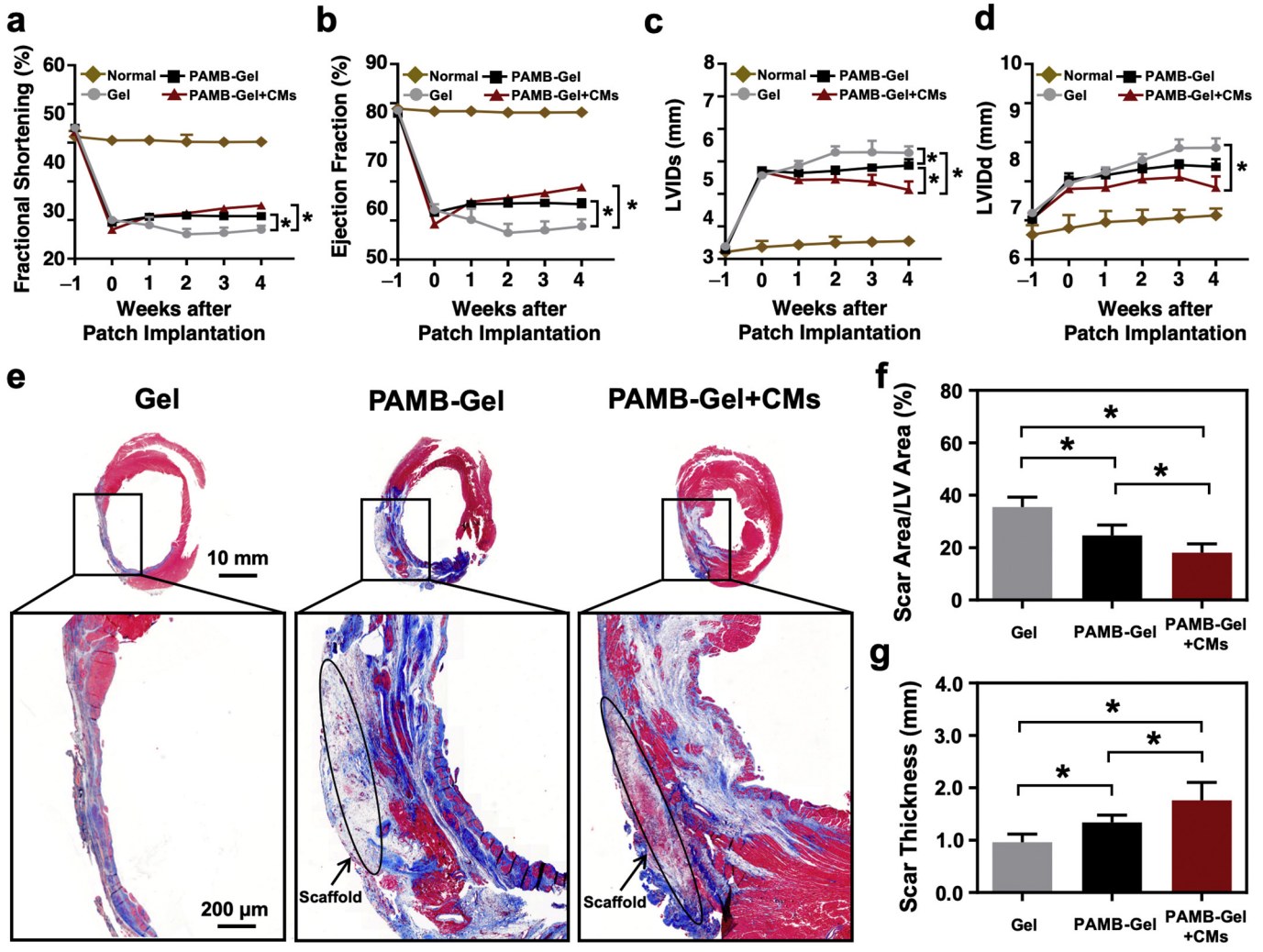

Fig. 6. Echocardiograph at four weeks post-patch implantation, demonstrating that PAMB-Gel and PAMB-Gel + CMs patches had greater (a) fractional shortening and (b) ejection fraction but smaller (c) LVIDs and (d) LVIDd than Gel patch ($n = 6$ in each of Gel and PAMB-Gel groups, $n = 4$ in each of normal and PAMB-Gel + CMs groups). (e) Representative histological images of staining with Masson's Trichrome of cross-sectioned hearts excised four weeks after patch implantation. (f) Scar size and (g) scar thickness of each studied group (n = 6 in each of Gel and PAMB-Gel groups, n = 4 in PAMB-Gel + CMs group). *$P < 0.05$.

host myocardia, retained their thickness (Fig. 6e). Notably, the scars were significantly smaller and substantially thicker in the bioengineered patch-treated group than in the Gel patch-treated group or the PAMB-Gel patch-treated group ($P < 0.05$, Fig. 6f and g), revealing that CM transplantation has great potential for the repair of injured cardiac tissues. Additionally, we observed a large number of viable CMs that were originally seeded within the scaffold at four weeks after the patch implantation (Fig. 6e), facilitating a significantly more reduction in infarct size (Fig. 6f) and a greater preservation of scar thickness (Fig. 6g) in the PAMB-Gel + CM group as compared to the PAMB-Gel group.

The application of the as-proposed conductive PAMB-Gel patch has the advantages of both supporting for cardiomyocyte survival (Fig. 3b) and enhancing electrical activity (Figs. 3f–h and 4b–d). The patch effectively increased impulse propagation through the infarcted zone and permitted appropriately timed contraction of viable myocardium isolated by the infarct scar (Fig. 5e), thereby facilitating the improvement of cardiac function. Furthermore, our data demonstrated that this bioengineered conductive patch (PAMB-Gel + CMs) exhibited more effective synergistic functional improvement and greater reduction of adverse cardiac remodeling when compared with other patches in our animal model (Fig. 6a–g).

4. Conclusions

In conclusion, a novel bioengineered conductive patch was developed from a gelatin-based gelfoam that had been conjugated with a conductive polymer PAMB. This three-dimensional, porous patch supported CM engraftment and cell survival and synchronized CM beating as well as enhanced conduction velocity in CMs. *In vivo* implantation of the bioengineered conductive patch over the infarcted heart improved electrical impulse propagation across the scarred tissue and electrically activated isolated contracting regions to bridge the scar barrier to the healthy myocardium. This newly developed bioengineered conductive patch represents an important advance with great potential as a new treatment for heart disease-related conduction abnormalities.

Supplementary data to this article can be found online at https://doi.org/10.1016/j.jconrel.2020.01.027.

Acknowledgments

This work was supported by a grant from the Canadian Institutes of Health Research (332652 awarded to R.-K. L) and grants from the Ministry of Science and Technology (MOST 107-3017-F-007-002) and the Ministry of Education (MOE 107QR001I5) of Taiwan, ROC.

References

[1] World Health Organization, World health statistics 2017: Monitoring health for the SDGs sustainable development goals, World Health Organization, 2017.
[2] Y. Sun, K.T. Weber, Infarct scar: a dynamic tissue, Cardiovasc. Res. 46 (2000) 250–256.
[3] P. Menasche, A.A. Hagege, J.T. Vilquin, M. Desnos, E. Abergel, B. Pouzet, A. Bel, S. Sarateanu, M. Scorsin, K. Schwartz, P. Bruneval, M. Benbunan, J.P. Marolleau, D. Duboc, Autologous skeletal myoblast transplantation for severe postinfarction left ventricular dysfunction, J. Am. Coll. Cardiol. 41 (2003) 1078–1083.
[4] A.A. Rane, K.L. Christman, Biomaterials for the treatment of myocardial infarction: a 5-year update, J. Am. Coll. Cardiol. 58 (2011) 2615–2629.
[5] T. Eschenhagen, C. Fink, U. Remmers, H. Scholz, J. Wattchow, J. Weil, W. Zimmermann, H.H. Dohmen, H. Schafer, N. Bishopric, T. Wakatsuki, E.L. Elson, Three-dimensional reconstitution of embryonic cardiomyocytes in a collagen matrix: a new heart muscle model system, FASEB J. 11 (1997) 683–694.
[6] R.K. Li, Z.Q. Jia, R.D. Weisel, D.A. Mickle, A. Choi, T.M. Yau, Survival and function of bioengineered cardiac grafts, Circulation 100 (1999) II63–II69.
[7] K.L. Christman, H.H. Fok, R.E. Sievers, Q. Fang, R.J. Lee, Fibrin glue alone and skeletal myoblasts in a fibrin scaffold preserve cardiac function after myocardial infarction, Tissue Eng. 10 (2004) 403–409.
[8] T. Sakai, R.K. Li, R.D. Weisel, D.A. Mickle, E.T. Kim, Z.Q. Jia, T.M. Yau, The fate of a tissue-engineered cardiac graft in the right ventricular outflow tract of the rat, J. Thorac. Cardiovasc. Surg. 121 (2001) 932–942.
[9] B.D. Polizzotti, S. Arab, B. Kühn, Intrapericardial delivery of gelfoam enables the targeted delivery of periostin peptide after myocardial infarction by inducing fibrin clot fomration, PLoS One 7 (2012) e36788.
[10] K. Kang, L. Sun, Y. Xiao, S.H. Li, J. Wu, J. Guo, S.L. Jiang, L. Yang, T.M. Yau, R.D. Weisel, M. Radisic, R.K. Li, Aged human cells rejuvenated by cytokine enhancement of biomaterials for surgical ventricular restoration, J. Am. Coll. Cardiol. 60 (2012) 2237–2249.
[11] C.C. Huang, H.W. Tsia, W.Y. Lee, W.W. Lin, D.Y. Chen, Y.W. Hung, J.W. Chen, S.M. Hwang, Y. Chang, H.W. Sung, A translational approach in using cell sheet fragments of autologous bone marrow-derived mesenchymal stem cells for cellular cardiomyoplasty in a porcine model, Biomaterials 34 (2013) 4582–4591.
[12] J. Wang, F. Guo, M. Yu, L. Liu, F. Tan, R. Yan, N. Li, Rapamycin/DiR loaded lipid-polyaniline nanoparticles for dual-modalimaging guided enhanced photothermal and antiangiogeniccombination therapy, J. Control. Release 237 (2016) 23–34.
[13] Y. Liu, J. Hu, X. Zhuang, P. Zhang, Y. Wei, X. Wang, X. Chen, Synthesis and characterization of novel biodegradable and electroactive hydrogel based on aniline oligomer and gelatin, Macromol. Biosci. 12 (2012) 241–250.
[14] J. Guan, J.J. Stankus, W.R. Wagner, Biodegradable elastomeric scaffolds with basic fibroblastgrowth factor release, J. Control. Release 120 (2007) 70–78.
[15] M.V. Risbud, A.A. Hardikar, S.V. Bhat, R.R. Bhonde, pH-sensitive freeze-dried chitosan-polyvinyl pyrrolidone hydrogels as controlled release system forantibiotic delivery, J. Control. Release 68 (2000) 23–30.
[16] H.G. Yi, Y.J. Choi, K.S. Kang, J.M. Hong, R.G. Pati, M.N. Park, I.K. Shim, C.M. Lee, S.C. Kim, A 3D-printed local drug delivery patch for pancreatic cancergrowth suppression, J. Control. Release 238 (2016) 231–241.
[17] X.Q. He, M.S. Chen, S.H. Li, S.M. Liu, Y. Zhong, H.Y.M. Kinkaid, W.Y. Lu, R.D. Weisel, R.K. Li, Co-culture with cardiomyocytes enhanced the myogenic conversion of mesenchymal stromal cells in a dose-dependent manner, Mol. Cell. Biochem. 339 (2010) 89–98.
[18] J. Abbott, T. Ye, L. Qin, M. Jorgolli, R.S. Gertner, D. Ham, H. Park, CMOS nanoelectrode array for all-electrical intracellular electrophysiological imaging, Nat. Nanotechnol. 12 (2017) 460–466.
[19] T.J. Herron, P. Lee, J. Jalife, Optical imaging of voltageand calcium in cardiac cells & tissues, Circ. Res. 110 (2012) 609–623.
[20] C. O'Shea, A.P. Holmes, T.Y. Yu, J. Winter, S.P. Wells, J. Correia, B.J. Boukens, J.R. De Groot, G.S. Chu, X. Li, G.A. Ng, P. Kirchhof, L. Fabritz, K. Rajpoot, D. Pavlovic, ElectroMap: high-throughput open-source software for analysis and mapping of cardiac electrophysiology, Sci. Rep. 9 (2019) 1389.
[21] Z. Cui, N.C. Ni, J. Wu, G.Q. Du, S. He, T.M. Yau, R.D. Weisel, H.W. Sung, R.K. Li, Polypyrrole-chitosan conductive biomaterial synchronizes cardiomyocyte contraction and improves myocardial electrical impulse propagation, Theranostics 8 (2018) 2752–2764.
[22] H. Morita, S. Nagase, K. Kusano, T. Ohe, Spontaneous T wave alternans and premature ventricular contractions during febrile illness in a patient with Brugada syndrome, J. Cardiovasc. Electrophysiol. 13 (2002) 816–818.
[23] H.J. Wellens, Value and limitations of programmed electrical stimulation of the heart in the study and treatment of tachycardias, Circulation 5 (1978) 845–853.
[24] T. Nguyen, E. El Salibi, J.L. Rouleau, Postinfarction survival and inducibility of ventricular arrhythmias in the spontaneously hypertensive rat: effects of ramipril and hydralazine, Circulation 98 (1998) 2074–2080.
[25] S. Miyagawa, Y. Sawa, S. Sakakida, S. Taketani, H. Kondoh, I.A. Memon, Y. Imanishi, T. Shimizu, T. Okano, H. Matsuda, Tissue cardiomyoplasty using bioengineeredcontractile cardiomyocyte sheets to repair damaged myocardium: their integration with recipient myocardium, Transplantation 80 (2005) 1586–1595.
[26] C.A. Thompson, B.A. Nasseri, J. Makower, S. Houser, M. McGarry, T. Lamson, I. Pomerantseva, J.Y. Chang, H.K. Gold, J.O. Vacanti, S.N. Oesterle, Percutaneous transvenous cellular cardiomyoplasty. A novel nonsurgical approach for myocardial cell transplantation, J. Am. Coll. Cardiol. 41 (2003) 1964–1971.
[27] C. Le Visage, O. Gournay, N. Benguirat, S. Hamidi, L. Chaussumier, N. Mougenot, J.A. Flanders, R. Isnard, J.B. Michel, S. Hatem, D. Letourneur, F. Norol, Mesenchymal stem cell delivery into rat infarcted myocardium usinga porous polysaccharide-based scaffold: a quantitative comparison withendocardial injection, Tissue Eng. A 18 (2012) 35–44.
[28] E.C. Perin, G.V. Silva, J.A.R. Assad, D. Vela, L.M. Buja, A.L.S. Sousa, S. Litovsky, J. Lin, W.K. Vaughn, S. Coulter, M.R. Fernandes, J.T. Willerson, Comparison of intracoronary and transendocardial delivery of allogeneic mesenchymal cells in a canine model of acute myocardial infarction, J. Mol. Cell. Cardiol. 44 (2008) 486–495.
[29] F. Wang, J. Guan, Cellular cardiomyoplasty and cardiac tissue engineering for myocardial therapy, Adv. Drug Deliv. Rev. 62 (2010) 784–797.
[30] T. Hagiwara, T. Demura, K. Iwata, Synthesis and properties of electrically conducting polymers from aromatic aminea, Synth. Met. 18 (1987) 317–322.
[31] J.S. Park, D.G. Woo, B.K. Sun, H.M. Chung, S.J. Im, Y.M. Choi, K. Park, K.M. Huh, K.H. Park, In vitro and in vivo test of PEG/PCL-based hydrogel scaffold for cell delivery application, J. Control. Release 124 (2007) 51–59.
[32] S. Yang, L. Jang, S. Kim, J. Yang, K. Yang, S.W. Cho, J.Y. Lee, Polypyrrole/alginate hybrid hydrogels: electrically conductive and soft biomaterials for human mesenchymal stem cell culture and potential neural tissue engineering applications, Macromol. Biosci. 16 (2016) 1653–1661.
[33] S.C. Kim, J. Whitten, J. Kumar, F.F. Bruno, L.A. Samuelson, Self-doped carboxylated polyaniline: effect of hydrogen bonding on the doping of polymers, Macromol. Res. 17 (2009) 631–637.
[34] W. Wang, B. Tan, J. Chen, R. Bao, X. Zhang, S. Liang, Y. Shang, W. Liang, Y. Cui, G. Fan, H. Jia, W. Liu, An injectable conductive hydrogel encapsulating plasmid DNA-eNOs and ADSCs for treating myocardial infarction, Biomaterials 160 (2018) 69–81.
[35] A.M. Martins, G. Eng, S.G. Caridade, J.F. Mano, R.L. Reis, G. Vunjak-Novakovic, Electrically conductive chitosan/carbon scaffolds for cardiac tissue engineering, Biomacromolecules 15 (2014) 635–643.
[36] D.A. Stout, J. Yoo, A.N. Santiago-Miranda, T.J. Webster, Mechanism of greater cardiomyocytes functions on conductive nanoengineered composites for cardiovascular applications, Int. J. Nanomedicine 7 (2012) 5653–5669.
[37] A.W. Smith, C.E. Segar, P.K. Nguyen, M.R. MacEwan, I.R. Efimov, D.L. Elbert, Long-term culture of HL-1 cardiomyocytes in modular poly(ethylene glycol) microsphere-based scaffolds crosslinked in the phase-separated state, Acta Biomater. 8 (2012) 31–40.
[38] K.I. Lie, H.J.J. Wellens, R.M. Schuilenburg, D. Durrer, Mechanisms and significance of widened QRS complexes during complete atrioventricular block in acute inferior myocardial infarction, Am. J. Cardiol. 33 (1974) 833–839.
[39] C.M. Ripplinger, Q. Lou, W. Li, J. Hadley, I.R. Efimov, Panoramic imaging reveals basic mechanisms of induction and termination of ventricular tachycardia in rabbit heart with chronic infarction: implications for low-voltage cardioversion, Heart Rhythm. 6 (2009) 87–97.